UNIVERSITYOF BIRMINGHAM

University of Birmingham Research at Birmingham

The actin cytoskeleton modulates the activation of iNKT cells by segregating CD1d nanoclusters on antigen-presenting cells

Torreno-Pina, Juan A; Manzo, Carlo; Salio, Mariolina; Aichinger, Michael C; Oddone, Anna; Lakadamyali, Melike; Shepherd, Dawn; Besra, Gurdyal S; Cerundolo, Vincenzo; Garcia-Parajo, Maria F

Document Version
Peer reviewed version

[Link to publication on Research at Birmingham portal](#)

Classification: Biological Sciences: Biophysics and Computational Biology; Immunology and Inflammation.

The actin cytoskeleton modulates the activation of invariant NKT cells by segregating CD1d nanoclusters on antigen presenting cells

Juan A. Torreno-Pina[a], Carlo Manzo[a], Mariolina Salio[b], Michael Aichinger[b,c], Anna Oddone[a], Melike Lakadamyali[a] Dawn Shepherd[b], Gurdyal S. Besra[d], Vincenzo Cerundolo[b,1,*] and Maria F. Garcia-Parajo[a,e,1,*]

[a]ICFO – Institut de Ciencies Fotoniques, The Barcelona Institute of Science and Technology, 08860 Castelldefels (Barcelona), Spain.

[b]MRC Human Immunology Unit, Weatherall Institute of Molecular Medicine, Radcliffe Department of Medicine, OX3 9DS, University of Oxford, United Kingdom.

[c]Present Address: EveliQure Biotechnologies GmbH, Campus Vienna Biocenter, Helmut-Qualtinger-Gasse 2, Staircase 1, 3rd floor, A-1030 Vienna, Austria.

[d]School of Biosciences, University of Birmingham, Edgbaston, Birmingham, B11 2TT, UK.

[e]ICREA-Institució Catalana de Recerca i Estudis Avançats, 08010 Barcelona, Spain.

[1]V.C. and M.F.G-P. contributed equally to this work.

*To whom correspondence should be addressed: vincenzo.cerundolo@imm.ox.ac.uk or maria.garcia-parajo@icfo.es

Corresponding author:

Prof. Maria F. Garcia-Parajo, ICFO-Institute of Photonic Sciences, Mediterranean Technology Park, 08860 Castelldefels (Barcelona), Spain.

Phone: +34-93-5534158; Fax: +34-93- 5534000; e-mail: maria.garcia-parajo@icfo.es

Manuscript information:	Number of text pages, main manuscript: 25
	Number of main figures: 7
	Number of tables: none
	Number of Supplementary figures: 5
	Number of Supplementary movies: 4

Keywords: Protein nanoclustering; single particle tracking; STED nanoscopy; iNKT cell autoreactivity

Short title: CD1d clustering regulates iNKT cell activation

Abstract

Invariant natural killer T cells (iNKT cells) recognize endogenous and exogenous lipid antigens presented in the context of CD1d molecules. The ability of iNKT cells to recognize endogenous antigens represents a distinct immune recognition strategy, which underscores the constitutive memory phenotype of iNKT cells and their activation during inflammatory conditions. However, the mechanisms regulating such 'tonic' activation of iNKT cells remain unclear. Here we show that the spatiotemporal distribution of CD1d molecules on the surface of antigen presenting cells (APCs) modulates activation of iNKT cells. By using super-resolution microscopy, we demonstrate that CD1d molecules form nanoclusters at the cell surface of APCs, whose size and density is constrained by the actin cytoskeleton. Dual color single particle tracking revealed that diffusing CD1d nanoclusters are actively arrested by the actin cytoskeleton preventing their further coalescence. Formation of larger nanoclusters occurs in the absence of interactions between CD1d cytosolic tail and the actin cytoskeleton and correlates with enhanced iNKT cell activation. Importantly, and consistently with iNKT cell activation during inflammatory conditions, exposure of APCs to the TLR7/8 agonist R848 increases nanocluster density and iNKT cell activation. Overall, these results define a novel mechanism that modulates iNKT cell autoreactivity based on the tight control by the APC cytoskeleton of the sizes and densities of endogenous antigen loaded CD1d nanoclusters.

Significance Statement

Invariant natural killer T (iNKT) cells react against CD1d-antigen presenting cells (APCs) in the absence of exogenous antigens, a feature defined as autoreactivity. How iNKT cell autoreactivity is fine-tuned to prevent autoimmunity remains enigmatic. Here we demonstrate that iNKT cell activation is regulated by the lateral nanoscale organization of CD1d loaded with exogenous and endogenous antigens. Using a combination of advanced biophysical techniques we show that CD1d molecules organize in nanoclusters on the membrane of APCs. We further discover that the actin cytoskeleton prevents enhanced CD1d nanoclustering by hindering physical encountering between CD1d diffusing nanoclusters, reducing basal iNKT cell activation. As such, regulation of CD1d nanoclustering through the actin cytoskeleton constitutes a novel mechanism to fine-tune peripheral iNKT cell autoreactivity.

\body

Introduction

It is well established that different populations of T lymphocytes can recognize not only peptides in the context of MHC class I and class II molecules, but also foreign and self-lipids in association with CD1 proteins(1), antigen-presenting molecules which share structural similarities with MHC-class I molecules. Of the five CD1 isoforms, CD1d restricts the activity of a family of cells known as invariant Natural Killer T (iNKT) cells, because of their semi-invariant T Cell Receptor (TCR) usage(1). To date, the exogenous glycolipid α-GalactosylCeramide (α-GalCer) represents the best characterized CD1d-restricted agonist for iNKT cells(2). Unlike conventional peptide specific T cells, iNKT cells react against CD1d$^+$ antigen presenting cells (APCs) in the absence of exogenous antigens, a feature defined as autoreactivity(3). iNKT cell autoreactivity underpins the constitutive memory phenotype of iNKT cells and their ability to be activated during a variety of immune responses, from infections to cancer and autoimmunity(1). Some of the endogenous antigens known to elicit iNKT cell autoreactivity belong to glycosphingolipid families, with a mix of α- and β-anomeric configurations (4-7). How iNKT cell autoreactivity is fine-tuned to prevent autoimmunity is subject of much investigation. Previous results have shown that exposure of APCs to TLR agonists enhances iNKT cell autoreactivity (8, 9), consistent with the proposed mechanism by which ligand availability is regulated by lysosomal glycosidases (4, 6).

The recent application of advanced optical techniques(10-13) in combination with substrate patterning and functionalization(14, 15) is providing detailed information on how the lateral organization of a variety of molecules located on both sides of the immunological synapse contributes to controlling T cell activation. Specifically, single molecule dynamic approaches and super-resolution optical nanoscopy experiments have provided indisputable proof that many receptors on the cell membrane organize in small nanoclusters prior to ligand activation(16). Membrane nanodomains enriched in cholesterol and sphingolipids(17), protein-protein interactions(18) and interactions between transmembrane proteins and the cytoskeleton(19, 20) have been all implicated in regulating receptor dynamics and nanoclustering. An emerging concept attributes the actin cytoskeleton the ability of imposing barriers or fences on the cell membrane restricting the lateral mobility of transmembrane proteins (19-21). This transient restriction would in turn increase the local concentration of transmembrane proteins leading to protein nanoclusters. For instance, it has been shown that the actin cytoskeleton promotes the dimerization rate of EGF receptors and facilitates ligand binding and signaling activation (18, 22). Confinement of CD36 has also been observed as a result of its diffusion along linear channels dependent on the integrity of the cortical cytoskeleton(23). This constrained diffusion promotes CD36 clustering, influencing CD36-mediated signaling and internalization. A similar mechanism has been proposed for the maintenance of MHCI clusters on the cell membrane by the actin cytoskeleton, with loss of MHCI clustering resulting in a decreased CD8-T Cell activation(24, 25).

Recent confocal microscopy studies have revealed that the association between agonist loaded-CD1d molecules and lipid rafts might contribute to the regulation of iNKT cell activation(26). This elegant study for the first time linked the spatial organization of CD1d molecules on the cell

5

membrane of APCs with the activation profile of iNKT cells. However, it remains unclear whether the results of these experiments obtained using mouse cells can be extended to human cells and whether further insights can be obtained by using higher resolution microscopy. Indeed, it is not yet known whether surface expressed CD1d molecules exist as monomers or as nanoclusters, and whether the actin cytoskeleton might regulate CD1d lateral organization and iNKT cell activation. Interestingly, it has been recently reported that the actin cytoskeleton impairs antigen presentation by CD1d and that disruption of F-actin or inhibition of the Rho-associated protein kinase enhances CD1d-mediated antigen presentation (27). These results suggest that the actin cytoskeleton might regulate, in a not yet known manner, antigen presentation by CD1d molecules.

Here, we combined dual-color single molecule dynamic approaches with super-resolution optical nanoscopy to characterize for the first time the spatiotemporal behavior of CD1d on living human myeloid cells. We find that α-GalCer loaded human CD1d (hCD1d) molecules are organized in nanoclusters on the cell membrane of APCs. We report that the actin cytoskeleton prevents enhanced hCD1d nanoclustering by hindering physical encountering between hCD1d diffusing nanoclusters, thus reducing basal iNKT cell activation. Furthermore, we observed an increase in nanocluster density upon activation of APCs with inflammatory stimuli, such as Toll like receptor (TLR) stimulation, mirroring the increased iNKT cell stimulation. Notably, even during inflammation the actin cytoskeleton retains an important role to limit hCD1d cluster size and iNKT cell activation. Overall, our results suggest that regulation of CD1d nanoclustering through the actin cytoskeleton represents a novel mechanism to fine tune peripheral iNKT cell autoreactivity.

Results

The actin cytoskeleton regulates the mobility of α-GalCer loaded hCD1d molecules

To study the lateral behavior of hCD1d on the cell membrane of APCs, we first performed high-speed single particle tracking (SPT) on the human myelomonocytic cell line THP-1, transduced with lentiviral vectors encoding hCD1d molecules and pulsed with the iNKT cell agonist α-GalCer. α-GalCer loaded hCD1d molecules were labeled at low density using a conjugate consisting of a biotinylated iNKT- T cell receptor (iNKT-TCR) (9, 28) and a streptavidin (SAV) coated quantum dot (QD655) (Fig. 1A). To ensure a single iNKT-TCR per QD, the iNKT-TCR-QD conjugate was prepared in an excess of free biotin to occlude SAV-QD excess binding sites. As further control to rule out any potential cross-linking effects induced by the SAV-QD multivalency, we also used the α-GalCer-hCD1d specific Fab fragment (Fab9b)(9, 28, 29) covalently attached to the small dye Atto647N. As a third control for the iNKT-TCR probe, α-GalCer loaded hCD1d molecules were labeled using a monovalent anti-CD1d antibody (CD1d42) conjugated to a QD under excess of free biotin. THP-1 cells were imaged on the ventral side using total internal reflection fluorescence microscopy (TIRFM). Individual features were detected and tracked to generate mobility trajectories (Fig. 1B). Individual trajectories were analyzed by deriving their instantaneous diffusion coefficients at short diffusion times (time lags 2 to 4, i.e., 20ms) D_{2-4} (Fig. 1C-F). The median D_{2-4} from multiple trajectories of α-GalCer loaded hCD1d molecules labeled with the iNKT-TCR-QD conjugate on different cells was 0.029 μm^2/s (Fig. 1C). Similar diffusion profiles and median diffusion coefficients were obtained with Fab9b-Atto647N (Fig. 1C) or when labeling α-GalCer loaded hCD1d using the

monovalent CD1d42-QD Ab (Fig. S1*A*). Altogether, these controls demonstrate that the lateral mobility of α-GalCer loaded hCD1d molecules is not affected by the iNKT-TCR-QD conjugate used throughout this study.

To address the potential role of the actin cytoskeleton in regulating the lateral mobility of hCD1d on the cell membrane of APCs, we treated THP-1 cells with the actin cytoskeleton-perturbing drug Cytochalasin D (CytoD)(20). CytoD treatment resulted in a nearly three-fold reduction in the instantaneous mobility of α-GalCer loaded hCD1d with a median D_{2-4} of 0.011 μm^2/s (Fig. 1*D*). Cell viability was not compromised under these conditions, as shown by propidium iodide staining (Fig. S1*B*)**.** Similar results were obtained when we followed the lateral mobility of α-GalCer loaded hCD1d molecules upon CytoD treatment using the monovalent CD1d42-QD Ab (Fig. S1*A*).

It has previously been shown that treatment of cells with a range of cytoskeleton perturbing drugs increases the instantaneous mobility of receptors, such as the FcεRI receptor(19) and the B-Cell receptor(20), which has been accounted for by the breaking of actin barriers that otherwise restrict the diffusion of receptors on the plasma membrane. To enquire whether the unexpected observed reduced mobility of hCD1d is specific or whether it results from an overall change of the membrane environment due to the CytoD treatment, we compared it with the mobility of CD71 molecules on THP-1 cells. In marked contrast to the behavior of hCD1d and consistent with the literature(30), treatment of THP1 cells with a similar concentration of CytoD led to a significant increase of CD71 diffusion (Fig. S1*C*), indicating that the observed reduced mobility of hCD1d is specific. Finally, to rule out any other potential secondary effects induced by CytoD, we measured the mobility of a cytoplasmic tail deleted hCD1d (TD-hCD1d) mutant, which lacks the final 10 amino acid residues including the AP-2 and AP-3 internalization motif and the lysine residue which is a target for ubiquitination(31). Similar to the results obtained with CytoD treated THP-1 cells, the mobility of the α-GalCer loaded TD-hCD1d mutant was three-fold lower than that of α-GalCer loaded wild type (WT) hCD1d (Fig. 1*D*).

Upon biosynthesis and egress from the ER, CD1d molecules reach the cell surface and continuously recycle through the endolysosomal compartment, where they sample different pools of self and foreign lipid antigens(32). While presentation of complex exogenous antigens requires CD1d molecules to traffic deep into the lysosomes(33), autoreactivity of human iNKT cells has been shown to have different requirements for CD1d lysosomal trafficking, possibly as a result of the different APCs used in the experiments (28, 34). To test whether these different trafficking pathways have an influence on the lateral mobility of hCD1d, we imaged unpulsed THP-1 cells and tracked hCD1d labeled with anti-CD1d42-QD (Fig. 1*A*). The instantaneous diffusion of control unpulsed WT-hCD1d molecules was approximately a factor of two lower than α-GalCer loaded molecules, with a median D_{2-4} value of 0.015μm^2/s (Fig. 1*E*). Interestingly, the lateral mobility of unpulsed WT-hCD1d was not affected by CytoD treatment (median D_{2-4}=0.017 μm^2/s), in strong contrast to the mobility reduction observed on α-GalCer loaded molecules after CytoD treatment. Moreover, the mobility of the unpulsed TD-hCD1d mutant was modestly reduced by 1.5-fold as compared to the WT counterpart (0.009 μm^2/s) (Fig. 1*E*). As such, these results show that unpulsed CD1d molecules are less sensitive to disruption of actin cytoskeleton interactions. Importantly, these data also indicate that the mobility of hCD1d differs depending on whether we sample molecules that have just reached the

cell surface from the ER (i.e., unpulsed and thus presenting self-lipids) or whether they have been recycling through the early and late endosomes.

To further strengthen these observations, we analyzed the lateral mobility of WT-hCD1d and TD-hCD1d molecules loaded with Gal(α1->2)GalCer (hereafter referred to as Gal-GalCer), which requires cleavage of the terminal galactose by α-galactosidase A in the lysosome for recognition by the iNKT-TCR(33). Recognition of this pool of hCD1d molecules by the iNKT-TCR-QD thus identifies a cohort of hCD1d molecules that has exclusively trafficked through the endolysosomes and recycled back to the cell surface. These experiments indicated that the lateral mobility of Gal-GalCer loaded hCD1d molecules was significantly reduced upon CytoD treatment or deletion of the cytosolic tail (Fig. 1*F*), in analogy to the results obtained for α-GalCer loaded hCD1d. Moreover, we also analyzed individual trajectories at longer times (over 250ms) to obtain further insight on the mobility of hCD1d molecules. Consistent with the reduction in the D_{2-4} values (instantaneous diffusion), the degree of anomalous diffusion at longer observation times increased for α-Galcer and the Gal-GalCer loaded hCD1d molecules, whereas no changes were observed in the unpulsed case (Fig. S2). Altogether, these results demonstrate that in the absence of interactions between the cytoplasmic tail of hCD1d and the actin cytoskeleton, the lateral mobility of hCD1d recycled through the endosomes is drastically reduced.

hCD1d molecules form nanoclusters on the surface of APCs whose properties depend on actin cytoskeleton interactions.

Previous reports indicate that the actin cytoskeleton regulates the lateral organization and nanoclustering of receptors on the cell membrane (23). Given the marked effect of the actin cytoskeleton and the cytoplasmic tail of hCD1d on the lateral mobility of hCD1d molecules that traffic through endosomes, we thought to visualize the nanoscale organization of hCD1d on the surface of THP-1 cells using stimulated emission depletion (STED) nanoscopy (35). STED images of anti-CD1d42 labeled hCD1d were performed on the dorsal side of fixed THP-1 cells. To avoid any potential artifacts related to CytoD treatment on the dorsal cell membrane morphology that could affect the quantification of STED images, we particularly focused on WT-hCD1d and the TD-hCD1d mutant since SPT experiments showed similar lateral diffusion of exogenous lipid-loaded (αGalCer and GalGalCer) TD-CD1d molecules and CytoD treated samples. Images were analyzed using a custom-made algorithm based on Bayesian inference of the fluorescence intensity distribution, improving data quantification and increasing the effective resolution beyond that of STED raw images (see Materials and Methods and Ref. 36). Interestingly, α-GalCer loaded WT-hCD1d molecules formed small nanoclusters on the surface of THP-1 cells with a median cluster size of 78 nm, containing 3.8 median number of hCD1d molecules/cluster (Fig. 2*A-C*) resulting in a nanocluster density of around 75 hCD1d/μm^2 (Fig. 2*D*). To verify that CD1d nanoclustering is real and not resulting from the enhanced expression of hCD1d on transduced THP-1 cells, we imaged hCD1d on blood-derived primary human CD14^{+} monocytes. Analysis of STED images confirmed the presence of hCD1d nanoclusters, albeit being smaller in size (49 nm as median cluster size) compared to THP-1 cells (Fig. S3). These data demonstrate that hCD1d forms nanoclusters on the plasma membrane of APCs.

Remarkably, α-GalCer loaded TD-hCD1d molecules, lacking the cytoplasmic tail, showed significantly larger and denser nanoclusters with a molecular density nearly three-fold higher (197 ± 17 hCD1d/μm^2) than α-GalCer loaded WT-hCD1d (Fig. 2A-D). A similar trend was equally observed for Gal-GalCer loaded TD-hCD1d. Indeed, larger nanoclusters (median cluster size of 93 nm, 8.2 median number of hCD1d molecules/cluster) and increased density (187 ± 12 hCD1d/μm^2) were measured compared to their WT-hCD1d counterparts (median cluster size of 80 nm, 3.3 median number of hCD1d molecules/cluster, 80 ± 6 hCD1d/μm^2) (Fig. 2A,E-G). These results show that the mobility reduction measured on the exogenous-loaded TD-CD1d molecules (Fig. 1D,F) is accompanied by an increased nanoclustering on the cell surface. In contrast, self-lipid loaded TD-hCD1d molecules displayed only slightly larger nanoclusters, in terms of size and number of molecules with no significant changes in nanocluster densities compared to self-lipid loaded WT-hCD1d molecules (Fig. 2A,H-J). These small changes in nanoclustering degree on unpulsed TD-hCD1d compared to WT-hCD1d are also consistent with the minor changes observed on their lateral mobility. Altogether, these results indicate once more that the effect of the cytoplasmic tail on hCD1d organization is predominantly on the pool of molecules that has trafficked through the lysosome.

Perturbation of the actin cytoskeleton increases dynamic encounters between α-GalCer loaded hCD1d nanoclusters

We hypothesized that the increased nanoclustering observed on α-GalCer loaded TD-hCD1d might result from dynamic encounters between individual nanoclusters that could favorably lead to local enrichment of hCD1d molecules in the absence of cytoskeleton interactions. To test this possibility in living cells we applied dual-color SPT. We labeled α-GalCer loaded hCD1d using iNKT TCRs coupled to two different QDs (Fig. 3A) at equimolar concentrations to increase the probability of detecting nanocluster interaction events (Fig. 3B, Movies S1-S3), while allowing for single pair trajectory recording. Two-dimensional trajectories of spatially close QDs (red and green) were generated (Fig. 3C) and their separation distance was plotted vs. time (Fig. 3D). In the case of truly interacting nanoclusters, their separation distances should remain small (close to the nanocluster size) for periods longer than random encounter events (22, 37). As expected, CytoD treatment of α-GalCer loaded WT-hCD1d and α-GalCer loaded TD-hCD1d showed significantly shorter separation distances over time compared to the untreated pulsed WT-hCD1d control (Fig. 3B,D,E) (median interparticle distance of 106 nm for CytoD treated cells, 130 nm for TD-hCD1d and 284 nm for the control case). These results were further validated by Monte-Carlo simulations of random encounters while accounting for the respective diffusion coefficients in the three different cases. The shorter distances experimentally obtained as compared to the simulations (Fig. 3E) confirm local enrichment of hCD1d nanoclusters upon perturbation of actin cytoskeleton interactions, following either CytoD treatment or removal of the hCD1d cytoplasmic tail. This sustained enrichment (lasting at least 1s in our experiments) would effectively increase hCD1d nanoclustering in the absence of actin cytoskeleton interactions, consistent with the super-resolution data.

The actin cytoskeleton spatiotemporally arrests diffusing α-GalCer loaded hCD1d nanoclusters on the cell membrane

The data presented so far indicate that the actin cytoskeleton somehow hinders dynamic interactions between hCD1d nanoclusters preventing their further coalescence into larger clusters.

To directly visualize how actin might accomplish such a role we performed dual-color TIRFM imaging of hCD1d and actin. We used hCD1d transduced THP-1 cells expressing lifeact-GFP, a fluorescent marker of F-actin(38). We labeled individual α-GalCer loaded hCD1d nanoclusters with the iNKT-TCR-QD conjugate and followed their lateral mobility with respect to actin, as previously reported for other cell membrane receptors(19, 20) (Fig. 4*A*). Individual trajectories of diffusing WT-hCD1d nanoclusters were reconnected and superimposed on the actin image (Fig. 4*B,C* and Movie S4). Interestingly, WT-hCD1d nanoclusters exhibited a highly restricted mobility in actin-rich regions (Fig. 4*B*). In contrast, WT-hCD1d mobility increased in actin-poor regions (Fig. 4*C*). These observations were substantiated by calculating the instantaneous mobility of a selected sub-population of individual trajectories that were found to diffuse inside and outside actin-rich regions. Indeed, WT-hCD1d nanoclusters displayed a remarkably slow diffusion inside actin-rich regions (median D_{2-4} = 0.0074 μm^2/s) compared to outside (median D_{2-4} = 0.025 μm^2/s) (Fig. 4*D*), revealing that the actin cytoskeleton arrests mobile α-GalCer loaded WT-hCD1d nanoclusters once they enter into actin-rich regions. In contrast, a similar analysis on a selection of α-GalCer loaded TD-hCD1d trajectories that diffused outside and inside actin-rich regions showed no significant difference in terms of their instantaneous diffusion (Fig. 4*D*), consistent with the observations that the mobility of the TD-mutant is not affected by the presence of the actin cytoskeleton (Fig. 1*D*).

To obtain a more robust quantification of the data we generated cartography maps of α-GalCer loaded WT-hCD1d and α-GalCer loaded TD-hCD1d superimposed on actin fluorescence images. These maps provide the spatial positions of hCD1d nanoclusters as they dynamically explore the cell membrane in relation to actin, with a localization accuracy of 20nm(37) (Fig. 4*E,F*). Cartography maps of α-GalCer loaded WT-hCD1d showed two different features: a) more dispersed localization positions outside actin regions resulting from its dynamic exploration of the cell membrane and; b) highly concentrated localization positions in actin-rich areas consistent with the arrest of the receptor in these regions (Fig. 4*E*). In contrast, no noticeable difference in terms of localization distribution with respect to actin was observed for α-GalCer loaded TD-hCD1d (Fig. 4*F*), already suggesting that the dynamic exploration of α-GalCer loaded TD-hCD1d is actin-independent. To quantify these differences we applied a custom-made algorithm that calculates the relative fraction of hCD1d localization positions as a function of actin intensity changes in different regions, Δactin (Fig. S4 and Materials and Methods). Positive values of Δactin represent actin-rich regions, while negative values reflect actin-poor regions. Δactin=0 corresponds to no actin intensity changes. Only THP-1 cells bearing similar expression levels of lifeact-GFP were used for the analysis. WT-hCD1d displayed a clear linear relationship between the number of localization positions and the amount of actin, with a positive slope of 0.34 ± 0.03, indicating that higher number of WT-hCD1d localization positions directly correlates with higher values of actin intensity (Fig. 4*G*). This increased number of spatial positions in actin-rich areas means that the receptor explores multiple times the same region, remaining spatiotemporally confined by actin. Together with the restricted mobility of WT-hCD1d observed on the actin-rich regions (Fig. 4*D*), these results prove that the actin cytoskeleton actively arrests WT-hCD1d nanoclusters on the cell membrane, preventing their further aggregation. In marked contrast, the number of localizations positions for TD-hCD1d shows only a weak dependence on actin (slope of 0.07 ± 0.08) (Fig. 4*G*) demonstrating no preferred interactions between TD-hCD1d and the actin cytoskeleton.

Perturbation of the actin cytoskeleton of APCs results in enhanced iNKT cell activation

Given that perturbing actin cytoskeleton interactions resulted in enhanced α-GalCer loaded hCD1d nanoclustering on APCs, we sought to address the consequences of such altered spatiotemporal organization on iNKT cell activation. For this, APCs were pulsed with different α-GalCer concentrations and treated with CytoD. APCs were then fixed and incubated with iNKT cells. IFN-γ production upon iNKT cell activation was measured by ELISA. Notably, CytoD-treated hCD1d-tranduced THP-1 cells (Fig. 5*A*) and CytoD-treated immature dendritic cells (Fig. 5*B*) elicited increased iNKT cell activation compared to APCs with an intact actin cytoskeleton. Moreover, this increase was more pronounced at low agonist concentrations. The increase in IFN-γ production was not due to increased hCD1d expression upon CytoD treatment (Fig. 5*C*). These results thus show that the actin cytoskeleton of APCs regulates the degree of iNKT cell activation. Interestingly, these data are fully in line with other reports where nanoclustering of antigen presenting proteins have been shown to enhance more effectively T cell activation at low agonist densities(39).

The actin cytoskeleton regulates hCD1d nanoclustering under inflammatory conditions

It has been described that innate stimuli, such as TLR stimulation, can trigger iNKT cell activation in a CD1d-dependent manner(8, 9, 28, 40). To test whether perturbation of the actin cytoskeleton of APCs exposed to inflammatory conditions also resulted in enhanced iNKT cell activation, we treated hCD1d transduced THP-1 cells with the TLR7/8 ligand R848. After CytoD treatment and fixation, APCs were incubated with iNKT cells. Increased IFN-γ production by R848-matured CytoD treated WT-hCD1d THP1 cells was observed, in line with the results with lipid pulsed cells (Fig. 5*D*). Moreover, increased IFN-γ production was hCD1d-dependent since blocking with an anti-CD1d Ab resulted in total abrogation of iNKT cell activation. Altogether these results strongly indicate that the actin cytoskeleton of APCs controls the activation of iNKT cells under innate and adaptive stimuli.

Since perturbation of the actin cytoskeleton of APCs resulted in enhanced iNKT cell activation upon R848 treatment of THP1 cells, we next addressed whether the interaction between the actin cytoskeleton and the cytoplasmic tail of hCD1d regulates hCD1d nanoclustering under inflammatory conditions as we have shown for α-GalCer loaded hCD1d. We stimulated both WT-hCD1d and TD-hCD1d transduced cells with the TLR7/8 ligand R848, performed STED nanoscopy (Fig. 6*A*) and analyzed hCD1d cluster size and composition. Interestingly, R848 stimulated WT-hCD1d formed smaller nanoclusters (47 nm as median cluster size) (Fig. 6*B*) than the unstimulated controls (77 nm as median cluster size). Moreover, those nanoclusters displayed a significantly higher number of hCD1d molecules (3.9 compared to 2.9 median number of unstimulated hCD1d molecules) (Fig. 6*C*) resulting in a strong increase of nanocluster density (180 ± 20 compared to 80 ± 5 hCD1d/μm^2) of WT-hCD1d molecules under inflammatory conditions (Fig. 6*D*). Moreover, R848 stimulated TD-hCD1d nanoclusters had a larger size (90 nm compared to 47 nm) (Fig. 6*E*) and contained a higher number of molecules (8.1 compared to 3.9 hCD1d molecules) (Fig. 6*F*) than the WT counterpart resulting in an increased nanocluster density of TD-hCD1d (231 ± 15 compared to 180 ± 20 hCD1d/μm^2) (Fig. 6*G*), in analogy with the results obtained with α-GalCer-TD-hCD1d (Fig. 2*E,F,G*).

These results highlight the important role of actin cytoskeleton interactions in controlling the extent of hCD1d nanoclustering on the cell membrane of APCs during inflammatory conditions. Moreover,

since hCD1d undergoes lysosomal trafficking under inflammatory conditions in analogy to α-GalCer pulsing(28), these data provide further support for the role of the interaction between the cytoplasmic tail of hCD1d and the actin cytoskeleton in modulating hCD1d nanoclustering after endosome recycling.

Discussion

We have for the first time characterized the spatiotemporal behavior of hCD1d on the surface of APCs at the nanoscale level. We found that hCD1d molecules organize in small nanoclusters on the cell membrane. Moreover, we observed that the actin cytoskeleton plays a major role in regulating the degree of hCD1d nanoclustering by segregating them away from each other. Treatment of THP-1 cells with CytoD or deletion of the hCD1d cytoplasmic tail led to larger nanoclusters and a concomitant reduction of hCD1d mobility. Furthermore, increased hCD1d nanoclustering directly correlated with enhanced iNKT cell activation. Notably, under inflammatory conditions hCD1d formed denser nanoclusters, whose organization also depended on the actin cytoskeleton. This is in remarkable analogy to the spatial organization of α-GalCer and Gal-GalCer loaded hCD1d molecules in THP-1 cells either treated with CytoD or expressing tail deleted hCD1d molecules. Altogether our results reveal a novel mechanism by which APCs regulate iNKT cell activation by fine-tuning the spatial organization of hCD1d on the cell membrane.

CD1d molecules are structurally related to the classical MHC-I complex(41). Using super-resolution near-field microscopy, clusters of MHC-I from 70-600 nm in size were observed on the plasma membrane of fibroblasts(42). More recently, it was shown that such nanoclustering strongly depends on the actin cytoskeleton, which acts as a barrier to spatially concentrate MHC-I molecules(24). Consistent with these observations, deletion of the cytoplasmic tail increased the lateral mobility of MHC-I(43). Clustering of MHC-II complexes on the plasma membrane of APCs has also been reported(44-46). Using SPT approaches, it was shown that MHC-II displays hop-diffusion on the cell membrane in a manner that it is dependent on the integrity of the actin cytoskeleton(47). Disruption of actin cytoskeleton interactions by either perturbing the actin network or by truncating the MHC-II cytoplasmic tail increased the mobility of MHC-II (47, 48). In these experiments, the lateral organization of MHC molecules also had an impact on the extent of T cell activation, with larger clusters enhancing peptide-specific T cell effector functions, particularly at low antigen density(39). Notably, the role of actin on the spatiotemporal organization of MHC-I and MHC-II on the cell membrane of APCs is markedly different from the results reported here for hCD1d molecules. While the actin cytoskeleton is essential to actively maintain the clustering of MHC-I and MHC-II, in the case of hCD1d molecules perturbation of the actin cytoskeleton leads to enhanced aggregation of hCD1d molecules. Consistent with these findings, and also in contrast to MHC-I and MHC-II, disruption of the actin cytoskeleton or deletion of the hCD1d cytoplasmic tail results in reduced mobility of hCD1d nanoclusters. Altogether our results indicate that hCD1d-mediated lipid antigen presentation is differently regulated at the cell surface of APCs as compared to MHC-restricted peptide presentation. We speculate that the contrasting role played by the actin cytoskeleton in regulating MHC and hCD1d nanoclustering reflects an important functional difference between conventional peptide-specific T cells and innate-like lipid specific T cells. Indeed, whereas peptide-specific MHC-I and MHC-II restricted T cells undergo extensive negative selection in the thymus(49) to eliminate the autoreactive peptide repertoire, peripheral iNKT cells retain the

ability to react to self-lipids presented by CD1d molecules. This so-called "autoreactivity by design"(3) underpins the essential immunoregulatory role of iNKT cells.

Much research is being undertaken to understand how iNKT cell autoreactivity in the periphery is fine-tuned to prevent overt autoimmunity. Initial results suggested that β-anomeric self-lipids were the main self-ligands recognized by the iNKT cell autoreactive response(4), and that a combination of increased lipid biosynthesis, increased CD1d expression and co-stimulatory cytokines was driving iNKT cell reactivity following APC activation(4, 8, 9). Co-stimulation by inflammatory cytokines is essential to achieve iNKT cell activation in these infectious settings, as extensive structural analysis revealed that the iNKT TCR interact with β-anomeric self-lipids CD1d complexes with low affinity(50). Recently, evidence has emerged for recognition of α-anomeric self-lipids bound to CD1d molecules(5, 6). As the affinity of the iNKT TCR for α-anomeric lipids is much higher than for β-anomeric CD1d-lipid complexes(50), an even tighter regulation of the availability of α-anomeric CD1d-lipid complexes is required. This is accomplished, for example, through the concerted action of biosynthetic and catabolic pathways, which in turn are modulated during inflammation(6). In addition to the affinity and CD1d occupancy of self-lipid antigens, our results underscore the importance of hCD1d clustering at the cell surface of APCs as a further mechanism to fine tune iNKT cell autoreactivity in peripheral tissues. Indeed, while at steady state the actin network plays an important role in limiting basal iNKT cell autoreactivity, the observed increase in hCD1d nanocluster density upon TLR stimulation suggests that the actin cytoskeleton might also regulate iNKT cell activation under inflammatory conditions, increasing the overall avidity of self-lipid loaded CD1d nanoclusters. This hypothesis is consistent with the previously reported increased staining of TLR-matured APCs with a soluble iNKT TCR detecting self-lipid CD1d complexes(9).

Endogenous lipid loaded CD1d molecules traffic from the ER to the cell surface via the Golgi system, where they acquire a variety of self-lipids(51). From the plasma membrane, CD1d molecules constitutively recycle through the endolysosomal compartment. A tyrosine based internalization motif in the cytoplasmic tail initiates clathrin dependent endocytosis, while association with the adaptor AP-2 and the Arf-like GTPase Arl8b control lysosomal trafficking(52). It has been previously reported that the association of exogenous lipid loaded CD1d with membrane lipid rafts on the plasma membrane of murine cells was dependent on the internal trafficking of CD1d molecules(26). Furthermore, it has also been shown that upon inflammatory stimuli, loading of self-lipids also requires trafficking of CD1d molecules through the lysosomal compartment(28). Our data extend these observations by demonstrating that regulation of hCD1d nanoclustering by the actin cytoskeleton selectively differs between hCD1d molecules presenting either exogenous lipids, such as α-GalCer and Gal-GalCer, or self-lipids under inflammatory conditions, and hCD1d molecules loaded with endogenous lipids hCD1d under resting conditions. These results are consistent with the hypothesis that regulation of hCD1d nanoclustering by the actin cytoskeleton selectively occurs on the pool of recycling hCD1d molecules that has trafficked backward and forward from the endolysosomal compartments to the cell surface, rather than on the pool of hCD1d reaching the cell surface directly from the endoplasmic reticulum. It will be of interest to investigate how the spatiotemporal behavior of hCD1d might also be affected by the absence of lysosomal lipid transfer proteins such as saposins, which have been shown to facilitate exogenous as well as self-lipid antigen presentation(28, 53).

The general consensus on the emerging role of the actin cytoskeleton in regulating cell membrane organization is that it restricts the lateral diffusion of transmembrane proteins by creating temporal physical barriers close to the cell membrane(19). These barriers locally confine membrane receptors increasing their local concentration and promoting clustering(23). In the case of hCD1d molecules, we observed similar arrest on its mobility in actin-rich regions. However, although hCD1d nanoclustering might be locally enhanced on certain hotspots of the cell membrane by actin, long-range hCD1d clustering is prevented by lowering the encountering probability of distant diffusing hCD1d nanoclusters. Thus, the actin cytoskeleton would effectively impose barriers and/or obstacles to the encountering of CD1d nanoclusters limiting their aggregation state. Removal of these fences by actin disruption would then favor the encountering of CD1d nanoclusters leading to larger clusters (Fig. 7). In support of this model we have performed super-resolution STORM imaging of the actin cytoskeleton on THP-1 cells before and after CytoD treatment (Fig. S5). While the intact actin cytoskeleton shows very fine structures with networks of tiny filaments and small compartments, treatment with CytoD led to a reduction of filament density and caused the formation of major actin aggregates separated by larger free spaces.

These results might bring new insights on how the actin cytoskeleton fine-regulates the lateral behavior of membrane proteins at multiple temporal and spatial scales. Recent results have shown the importance of ERM proteins in linking the transmembrane region of surface receptors, such as the BCR, to the actin cytoskeleton(20). Further experiments are warranted to assess whether this family of proteins is also controlling the interaction between the CD1d cytosolic tail and the cortical actin cytoskeleton. Consistent with this possibility, it has recently been shown that Rho kinase controls antigen presentation by CD1d molecules by prohibiting actin fiber de-polymerization(27).

In conclusion, our results highlight a novel mechanism that APCs employ to regulate lipid antigen presentation via CD1d molecules in order to modulate iNKT cell autoreactivity, a unique property that distinguishes this cell subset from conventional CD4$^+$and CD8$^+$ T cells. The observation that a similar actin-dependent mechanism regulates presentation of exogenous lipids and self-lipids upon inflammatory stimuli further adds to the uniqueness of the CD1d-iNKT cell system in bridging innate and adaptive immune responses. Moreover, this study underscores the importance of emerging concepts such as protein nanoclustering in deepening our understanding of how leukocytes can fine-tune at the molecular level the outcome of an immune reaction. We predict this type of studies will provide essential information for the future optimization of novel immune-based therapeutic strategies.

Materials and Methods

Antibodies and Reagents. Monoclonal mouse anti-human CD1d (CD1d42) and monoclonal mouse anti-human CD71 (clone M-A712) antibodies were purchased from BD Pharmingen. Poly-L-lysine (PLL), Cytochalasin D (CytoD), DMSO, Atto647N-NHS ester and di-thiothreithol (DTT) were purchased from Sigma Aldrich. Human fibronectin (FN) was purchased from Roche. Streptavidin coated QD655 and QD585, goat-anti-mouse Alexa Fluor 488 antibody (A-11001) and D-biotin were purchased from

Invitrogen. Maleimide-PEG2-Biotin and Slide-A-Lyzer MINI Dialysis Units were purchased from Thermo Scientific.

Cell Medium and specific reagents. The complete medium (CM) used throughout this study was RPMI 1640 (Gibco) for THP-1 and IMDM (Gibco) for iNKT cells. CM was supplemented with 2 mM L-glutamine, 1% non-essential amino acids, 1% sodium pyruvate, 1% pen/strep, 5 x10^{-5} 2ME (all from Gibco) and serum: 10% FCS (Sigma) for THP-1; 5% Human AB Serum (Sigma) for iNKT cells. Recombinant human IL-2 was produced in our laboratory as described(9).

Lipids: α-GalCer and Gal(α1$\rightarrow$2)GalCer were synthesized using strategies described previously(9) and their structures were confirmed by mass spectrometry. The dried lipids were dissolved at 10 mg/ml in a solution of chloroform:methanol:water (10:10:3; v/v/v), followed by dilution in 150mM NaCl, 0.5% Tween 20 (vehicle solution) at 100-200 μg/ml stock solution (depending on solubility). The solution was heated at 80°C for 5 minutes followed by sonication for 5 minutes in an ultrasonic water bath.

Soluble iNKT-TCR heterodimers were generated as described(9).

Generation of iNKT cells and Dendritic Cells. Blood was purchased from the UK National Blood Service. Human iNKT cells were isolated by cell sorting with CD1d-α-GalCer tetramers and/or Vα24 and Vβ11 antibodies (Immunotech, Marseille, France) directly from PBMC or after expansion with autologous DCs pulsed with α-GalCer as described(28). iNKT cells were grown in CM (containing 5% human AB serum instead of FCS) supplemented with 1000 U/ml IL-2 and periodically re-stimulated. Dendritic Cells (DCs) were differentiated from MACS-purified CD14 monocytes from healthy blood donors as described(9).

Generation of THP-1 cells over-expressing human CD1d constructs. Full length human CD1d was cloned in the pHR-SIN lentiviral vector. Lentivirus particles were made as described(28) and used to infect THP-1 cells (ATCC). Tail deleted (TD) human CD1d, lacking the last 10 AA, was cloned in the pHR-SIN lentiviral vector using a strategy previously described(28). THP1-CD1d cells were transduced with a lentivirus encoding lifeact GFP as previously described(9). GFP positive cells were enriched by cell sorting.

iNKT cell stimulation assays. imDCs and THP-1-CD1d cells were plated at 50000/well in U bottom 96 well plates and pulsed overnight at the indicated concentration of lipids. In some experiments, cells were matured for 36 hours with the TLR7/8 ligand R848 (Invivogen, 5-10 μg/ml). Cells were extensively washed, treated for 1 hour at 37ºC with CytoD used at 10μM in HBSS (Gibco) and immediately fixed in glutaraldehyde(9). Fixed APCs were used to stimulate iNKT cells (20000-30000/well in duplicate or triplicate). iNKT cell activation was assessed by IFN-γ ELISA (BD Pharmingen) on supernatants harvested after 36 hours. When indicated, blocking anti CD1d antibody (clone 42.1, BD Pharmingen) was added at 20μg/ml 30 min before adding iNKT cells. Viability of APCs and hCD1d expression after CytoD treatment was assessed by Flow cytometry upon staining with anti CD1d PE (BD Pharmingen) and propidium iodide (BD Pharmingen). Data were acquired on a Cyan DAKO flow cytometer and analyzed with Flowjo.

Labeling conjugates for SPT experiments in living cells. Monovalent anti-human CD1d or CD71 Abs were prepared from CD1d42 and CD71 Ab by reduction with dithiothreitol (DTT) following manufacturer's instructions. Reduced Abs were then biotinylated with Maleimide-PEG2-Biotin and quenched with Iodoacetamide. Unbound biotin was removed by overnight dialysis at 4ºC using Slide-A-Lyzer MINI Dialysis Units. To monitor each reaction step, a 4-12% Bis-Tris gel under denaturing and non-denaturing conditions was performed.

Biotinylated iNKT-TCR or monovalent Abs were mixed with streptavidine coated QD655 or QD585 in equimolar concentrations and stirred for at least 2h at 4ºC. Excess of free biotin was added to the solution to ensure a single iNKT-TCR (x10 excess biotin) or monovalent Ab (x50 excess biotin) per quantum dot.

Atto647N-NHS Ester labeling of the Fab9b (9, 29) was performed following manufacturer's instructions.

Single Particle Tracking. hCD1d transduced THP-1 cells were pulsed overnight with 50 ng/ml of α-GalCer or 400 ng/ml of Gal-GalCer. After 30 min of incubation on FN-coated coverslips at 37ºC and 5% CO_2, cells were labeled with 2nM of the iNKT-TCR-QD655 conjugate for 5 min at room temperature. Cells were then washed with cell medium three times to remove unbound iNKT-TCR-QD655 conjugates. When labeling the cells with antibody-derived probes, 2% human serum incubation was performed for 5 min at room temperature before adding monovalent antibodies or Fab fragments. Monovalent CD1d42-QD655 labeling was done at 0.2nM concentration. Fab9b-Atto647N labeling was done at 10nM concentration. On CytoD treated samples, treatment (10μM CytoD for 1 hour) was performed before labeling, on cells seeded on FN-coated coverslips for unpulsed hCD1d-THP-1 cells or after overnight pulsing with α-GalCer or Gal-GalCer. CytoD was maintained in the medium while imaging. CytoD controls were performed with DMSO diluted in the imaging medium with the same dilution used for CytoD experiments.

Fluorescence imaging was performed on the ventral side of the cell using a home-made single molecule sensitive microscope working under TIRF geometry. Continuous excitation of the QDs was provided by the 488-nm line of an Ar$^+$ laser (0.3kW/cm^2). Fluorescence was collected with a 1.4 NA oil immersion objective (Olympus) and guided into an EM-CCD camera (Hamamatsu) after suitable filtering. Movies were recorded at a frame rate of 100Hz for single QDs and 10Hz for Fab9b-Atto647N. For simultaneous dual-color measurements, the fluorescence emitted light was split and selected with appropriate dichroic mirror and filters and collected by the same EM-CCD camera (dual-color hCD1d imaging) or by a second intensified CCD Pentamax camera (dual-color hCD1d vs Lifeact-GFP imaging). Images of multi-fluorophore fluorescent beads (0.2 µm Tetraspeck, Invitrogen), having emission spectrum covering the two spectral windows were obtained to determine the spatial transformation leading to the overlay of the two spectral channels. To calculate the spatial transformation, at least 10 beads appearing on both channels were manually selected, their centroid positions calculated with subpixel accuracy and stored in two coordinate lists. The transformation matrix was inferred from the coordinate lists according to an affine transformation, correcting for displacement and small chromatic aberrations. For dual-color measurements of hCd1d, cells were labeled with an equimolar 2nM concentration of 2 conjugates: iNKT-TCR-QD655 and iNKT-TCR-QD585. Simultaneous dual-color images of QDs were performed at a

frame rate of 30Hz. Dual-color images of Lifeact-GFP and iNKT-TCR-QD655 were obtained on double transduced Lifeact-GFP & WT-hCD1d or TD-hCD1d THP-1 cells that had been pulsed overnight with 50 ng/ml of α-GalCer. Images were acquired at a frame rate of 60Hz. Under these imaging conditions, no changes in the actin cytoskeleton were observed and the actin intensity signal remained constant during the time of the experiments. Physiological conditions were maintained during the experiments using a temperature-controlled microincubation chamber (Warner Instruments) in combination with a constant 5% CO_2 supply (Okolab).

Single particle trajectory analysis. Trajectories of individual quantum dots with at least 100 points were reconnected with Matlab routines based on an algorithm described by Serge et al.(54) Trajectories of individual Fab9b-Atto647N were manually reconnected with a minimum trajectory length of 19 points.

Individual trajectories were analyzed by calculating their mean-squared-displacement (MSD) according to the following formula (55):

$$MSD_n \cdot \Delta t = \frac{1}{N-n-1} \sum_{j=1}^{N-n-1} \left(x_{j\Delta t + n\Delta t} - x_{j\Delta t} \right)^2 + \left(y_{j\Delta t + n\Delta t} - y_{j\Delta t} \right)^2 \qquad \text{(S1)}$$

where Δt is the time lag, N is the total number of frames of the trajectory, n represents the time increment and x,y represent the 2D particle position. Short-range diffusion coefficients were extracted from the linear fit to the 2nd- 4th point of the MSD curve using the following equation:

$$MSD = 4D_{2-4}t + \Delta_0 \qquad \text{(S2)}$$

where D_{2-4} is the instantaneous diffusion coefficient and Δ_0 is the MSD offset at zero time increment. The smallest detectable diffusion coefficient was obtained after imaging immobilized QDs or Atto647N dyes on a coverslip using TIRFM at the same frame rate as in the corresponding experiments, 100Hz and 10Hz respectively. Since in both cases, 95% of the immobile QDs displayed diffusion coefficients $<1\cdot10^{-3}$ μm^2/s, this value was considered as the threshold for discriminating immobile vs. mobile trajectories. To avoid any overestimation of the immobile fraction due to non-specific interaction of QDs or Atto647N dyes with the coverslip, only trajectories classified as mobile were used for the trajectory analysis.

Dual-color hCD1d trajectory analysis. Two-color QD tracking of labeled hCD1d (WT and TD) nanoclusters was performed at 2nM concentrations to increase the probability of finding nanocluster interaction events. Two-dimensional fluorescence trajectories of spatially close QDs (red: iNKT-TCR-QD655 and green: iNKT-TCR-QD585) were generated and the separation distance (interparticle distance) between QDs was determined from their dual-color pair trajectories by measuring the effective distance between the centroid positions of the diffusing QDs determined by fitting the point-spread function of the microscope with a Gaussian curve. Localization accuracy on the determination of the centroid position was 20nm for both colors. The initial QDs separation distance considered was 350nm and interparticle distances were calculated at every frame for a total observation time of 1s yielding 30 data points per QD pair. Interparticle distances of all pairs at every frame were collected into a histogram. Monte-Carlo simulations were performed to discriminate between random encounters of diffusing hCD1d nanoclusters or true enhanced interaction between hCD1d nanoclusters. 100 pairs of randomly diffusing nanoclusters were

simulated yielding 3000 simulated interparticle distances per simulated pair. The instantaneous diffusion coefficient for each experimental condition was used for simulating the dual-color trajectories.

Dual-color trajectory analysis of iNKT-TCR-QD labeled hCD1d on Lifeact-GFP labeled actin. A single Lifeact-GFP fluorescence image was bandpass-filtered in the frequency domain using standard ImageJ image processing. Only QDs that visited both low-actin and high-actin regions during the time course of an experiment (20s) were manually tracked. The trajectories were then divided into 10 points segments and the instantaneous diffusion coefficients of every segment were calculated as earlier described. The segments of the trajectories were visually classified to belong to either low-actin or high-actin regions after thresholding (>75%) the normalized Lifeact-GFP fluorescence images.

Generation of time-dependent membrane exploration maps. Time-dependent membrane exploration maps of iNKT-TCR-QD655 labeled hCD1d (WT and TD) with respect to actin were obtained as described in Torreno-Pina et al.(37). In brief, we first obtained dual-color TIRFM images of iNKT-TCR-QD655 and Lifeact-GFP, at a frame rate of 60Hz and for a total observation time of 1200 frames. The position of each single QD with 20nm localization accuracy was determined in every frame using a custom Matlab algorithm based on Serge et al.(54). The total number of QD localization positions in all the frames was then collapsed in one single image and overlaid into one single Lifeact-GFP fluorescence image. Cells with an actin cytoskeleton that did not change over the time course of an experiment were carefully selected for generating cartography maps.

Quantification of hCD1d localizations with respect to actin. Quantification of the data was performed by generating two concentric circles with different radii R_1 and R_2 (R_1=225 nm and R_2=1035 nm) and having each time a given localization of the cartography map as the center for both circles (Fig. S4). The total number of localizations enclosed in each circle was quantified; with N_1 being the total number of localizations enclosed by circle R_1 and N_2 = (# of localizations in R_2 − N_1). Moreover, the mean raw fluorescence intensity value of actin (A_1 and A_2 from R_1 and R_2, respectively) enclosed by each radius was also extracted from the superimposition of the circles on top of the actin image. This procedure was repeated by positioning the center of the two concentric circles at each hCD1d localization value. The behavior of WT-CD1d and TD-CD1d molecules with respect to the actin cytoskeleton was extracted by plotting the relative fraction of hCD1d localizations (N_1/N_2) against (A_1-A_2)/A_1=ΔActin. Only cells with a similar expression of lifeact-GFP were selected for this analysis.

Sample preparation for STED Nanoscopy. To avoid any potential artifacts due to CytoD treatment on membrane morphology that could affect the STED imaging, we exclusively focused on WT-hCD1d or TD-hCD1d transduced THP1 cells. WT-hCD1d or TD-hCD1d transduced THP1 cells were pulsed overnight with 100ng/ml α-GalCer or 400ng/ml Gal-GalCer. Alternatively, WT-hCD1d or TD-hCD1d transduced THP1 cells were stimulated with 10 µg/ml R-848 for 30h. Cells were then stretched on PLL-coated coverslips for 30 min at 37ºC and with 5% CO_2. After cell fixation with 2% paraformaldehyde, Fc-receptors were blocked with 2% human serum. CDd1 molecules on the cell membrane were labeled with 5µg/ml anti-CD1d42 Ab. Fluorescent secondary antibody labeling was

performed with a 5µg/ml goat anti-mouse Alexa Fluor 488-labeled antibody. Isotype controls were performed in order to test the specificity of the labeling procedure.

Stimulated Emission Depletion (STED) Nanoscopy. Confocal and STED images were obtained in a sequential manner using a 100x oil immersion objective (HCX PL APO 100x/1.4 Oil, Leica Microsystems, Germany) of a commercial CW-STED SP-7 microscope (Leica Microsystems, Germany). The STED laser intensity at the focal plane on the upper cell membrane was 130mW, and 1024x1024 pixels images were recorded at a scan speed of 1400Hz. In these conditions, no significant fluorescence photobleaching was observed. STED resolution was 85 nm as determined from the full-width-at half-maximum of sparse labeled Abs on glass by fitting the point-spread function of the STED microscope using a Lorentzian curve.

Analysis of the STED images. STED images were analyzed by means of a previously published algorithm based on Bayesian inference (36). The algorithm essentially relies on the detection of fluorescence features and their fitting as a sum of different point spread functions (PSFs) whose width and intensity distribution are estimated from images of sparse markers. For each image, the localization positions of all the retrieved PSFs were used to reconstruct an image that contains the molecular localizations belonging to each fluorescent feature of the raw STED image. The performance of such analysis has been previously tested on simulated images in a wide range of number densities, PSF widths and signal-to-noise ratio (SNR) (See SI text) (36). In our experimental conditions (number density=5-50 μm^{-2}, PSF width=85 nm, SNR=15-20 dB), the algorithm is able to retrieve a large percentage (>80%) of particles and to determine their location with high localization accuracy (~20 nm). Cluster size and number of hCD1d molecules per cluster were then calculated from the reconstructed images using the pair-correlation analysis (36). The pair-correlation function *g(r)* was calculated on reconstructed images obtained by convoluting the particle localizations with 2D Gaussian functions having width equal to the localization accuracies. Each curve represents the average of at least 30 pair correlations obtained over 3x3 μm^2 regions of interest.

References

1. Salio M, Silk JD, Yvonne Jones E, & Cerundolo V (2014) Biology of CD1-and MR1-Restricted T Cells. *Annu. Rev. Immunol.* 32:323-366.
2. Kawano T*, et al.* (1997) CD1d-restricted and TCR-mediated activation of Vα14 NKT cells by glycosylceramides. *Science* 278(5343):1626-1629.
3. Bendelac A, Bonneville M, & Kearney JF (2001) Autoreactivity by design: innate B and T lymphocytes. *Nat. Rev. Immunol.* 1(3):177-186.
4. Brennan PJ*, et al.* (2011) Invariant natural killer T cells recognize lipid self antigen induced by microbial danger signals. *Nat. Immunol.* 12(12):1202-1211.
5. Brennan PJ*, et al.* (2014) Activation of iNKT cells by a distinct constituent of the endogenous glucosylceramide fraction. *Proc. Natl. Acad. Sci. USA* 111(37):13433-13438.
6. Kain L*, et al.* (2014) The Identification of the Endogenous Ligands of Natural Killer T Cells Reveals the Presence of Mammalian α-Linked Glycosylceramides. *Immunity* 41(4):543-554.
7. Zhou D*, et al.* (2004) Lysosomal glycosphingolipid recognition by NKT cells. *Science* 306(5702):1786-1789.
8. Paget C*, et al.* (2007) Activation of invariant NKT cells by toll-like receptor 9-stimulated dendritic cells requires type I interferon and charged glycosphingolipids. *Immunity* 27(4):597-609.
9. Salio M*, et al.* (2007) Modulation of human natural killer T cell ligands on TLR-mediated antigen-presenting cell activation. *Proc. Natl. Acad. Sci. USA* 104(51):20490-20495.
10. Choudhuri K*, et al.* (2014) Polarized release of T-cell-receptor-enriched microvesicles at the immunological synapse. *Nature* 507:118-123.
11. Dustin ML & Depoil D (2011) New insights into the T cell synapse from single molecule techniques. *Nat. Rev. Immunol.* 11(10):672-684.
12. Vardhana S, Choudhuri K, Varma R, & Dustin ML (2010) Essential role of ubiquitin and TSG101 protein in formation and function of the central supramolecular activation cluster. *Immunity* 32(4):531-540.
13. Williamson DJ*, et al.* (2011) Pre-existing clusters of the adaptor Lat do not participate in early T cell signaling events. *Nat. Immunol.* 12(7):655-662.
14. Manz BN, Jackson BL, Petit RS, Dustin ML, & Groves J (2011) T-cell triggering thresholds are modulated by the number of antigen within individual T-cell receptor clusters. *Proc. Natl. Acad. Sci. USA* 108(22):9089-9094.
15. Mossman KD, Campi G, Groves JT, & Dustin ML (2005) Altered TCR signaling from geometrically repatterned immunological synapses. *Science* 310(5751):1191-1193.
16. Garcia-Parajo MF, Cambi A, Torreno-Pina JA, Thompson N, & Jacobson K (2014) Nanoclustering as a dominant feature of plasma membrane organization. *J. Cell Sci.* (127):4995-5005.
17. Lingwood D & Simons K (2010) Lipid rafts as a membrane-organizing principle. *Science* 327(5961):46-50.
18. Chung I*, et al.* (2010) Spatial control of EGF receptor activation by reversible dimerization on living cells. *Nature* 464(7289):783-787.
19. Andrews NL*, et al.* (2008) Actin restricts FceRI diffusion and facilitates antigen-induced receptor immobilization. *Nat. Cell Biol.* 10(8):955-963.
20. Treanor B*, et al.* (2010) The membrane skeleton controls diffusion dynamics and signaling through the B cell receptor. *Immunity* 32(2):187-199.
21. Morone N*, et al.* (2006) Three-dimensional reconstruction of the membrane skeleton at the plasma membrane interface by electron tomography. *J. Cell Biol.* 174(6):851-862.

22. Low-Nam ST*, et al.* (2011) ErbB1 dimerization is promoted by domain co-confinement and stabilized by ligand binding. *Nat. Struc. Mol. Biol.* 18(11):1244-1249.

23. Jaqaman K*, et al.* (2011) Cytoskeletal control of CD36 diffusion promotes its receptor and signaling function. *Cell* 146(4):593-606.

24. Lavi Y, Gov N, Edidin M, & Gheber LA (2012) Lifetime of major histocompatibility complex class-I membrane clusters is controlled by the actin cytoskeleton. *Biophys. J.* 102(7):1543-1550.

25. Segura J-M*, et al.* (2008) Increased mobility of major histocompatibility complex I-peptide complexes decreases the sensitivity of antigen recognition. *J. Biol. Chem.* 283(35):24254-24263.

26. Im JS*, et al.* (2009) Kinetics and cellular site of glycolipid loading control the outcome of natural killer T cell activation. *Immunity* 30(6):888-898.

27. Gallo RM*, et al.* (2012) Regulation of the actin cytoskeleton by rho kinase controls antigen presentation by CD1d. *J. Immunol.* 189(4):1689-1698.

28. Salio M*, et al.* (2013) Saposins modulate human invariant Natural Killer T cells self-reactivity and facilitate lipid exchange with CD1d molecules during antigen presentation. *Proc. Natl. Acad. Sci. USA* 110(49):E4753-E4761.

29. Denkberg G*, et al.* (2008) Phage display-derived recombinant antibodies with TCR-like specificity against α-galactosylceramide and its analogues in complex with human CD1d molecules. *Eur. J. Immunol.* 38(3):829-840.

30. Di Rienzo C, Gratton E, Beltram F, & Cardarelli F (2013) Fast spatiotemporal correlation spectroscopy to determine protein lateral diffusion laws in live cell membranes. *Proc. Natl. Acad. Sci. USA* 110(30):12307-12312.

31. Sugita M*, et al.* (2002) Failure of trafficking and antigen presentation by CD1 in AP-3-deficient cells. *Immunity* 16(5):697-706.

32. Moody DB & Porcelli SA (2003) Intracellular pathways of CD1 antigen presentation. *Nat. Rev. Immunol.* 3(1):11-22.

33. Prigozy TI*, et al.* (2001) Glycolipid antigen processing for presentation by CD1d molecules. *Science* 291(5504):664-667.

34. Chen X*, et al.* (2007) Distinct endosomal trafficking requirements for presentation of autoantigens and exogenous lipids by human CD1d molecules. *J. Immunol.* 178(10):6181-6190.

35. Hell SW (2007) Far-field optical nanoscopy. *Science* 316(5828):1153-1158.

36. Manzo C*, et al.* (2014) PSF decomposition of nanoscopy images via Bayesian analysis unravels distinct molecular organization of the cell membrane. *Sci. Rep.* 4: 4354, 2014.

37. Torreno-Pina JA*, et al.* (2014) Enhanced receptor–clathrin interactions induced by N-glycan–mediated membrane micropatterning. *Proc. Natl. Acad. Sci. USA* 111(30):11037-11042.

38. Riedl J*, et al.* (2008) Lifeact: a versatile marker to visualize F-actin. *Nat. Methods* 5(7):605-607.

39. Anderson HA, Hiltbold EM, & Roche PA (2000) Concentration of MHC class II molecules in lipid rafts facilitates antigen presentation. *Nat. Immunol.* 1(2):156-162.

40. Brigl M, Bry L, Kent SC, Gumperz JE, & Brenner MB (2003) Mechanism of CD1d-restricted natural killer T cell activation during microbial infection. *Nat. Immunol.* 4(12):1230-1237.

41. Moody DB, Zajonc DM, & Wilson IA (2005) Anatomy of CD1–lipid antigen complexes. *Nat. Rev. Immunol.* 5(5):387-399.

42. Hwang J, Gheber LA, Margolis L, & Edidin M (1998) Domains in cell plasma membranes investigated by near-field scanning optical microscopy. *Biophys. J.* 74(5):2184-2190.

43. Capps GG, Pine S, Edidin M, & Zúniga MC (2004) Short class I major histocompatibility complex cytoplasmic tails differing in charge detect arbiters of lateral diffusion in the plasma membrane. *Biophys. J.* 86(5):2896-2909.

44. Bosch B, Heipertz EL, Drake JR, & Roche PA (2013) Major histocompatibility complex (MHC) class II-peptide complexes arrive at the plasma membrane in cholesterol-rich microclusters. *J. Biol. Chem.* 288(19):13236-13242.

45. Fooksman DR (2014) Organizing MHC class II presentation. *Front. Immunol.* 5.

46. Turley SJ*, et al.* (2000) Transport of peptide-MHC class II complexes in developing dendritic cells. *Science* 288(5465):522-527.

47. Umemura YM*, et al.* (2008) Both MHC class II and its GPI-anchored form undergo hop diffusion as observed by single-molecule tracking. *Biophys. J.* 95(1):435-450.

48. Wade WF, Freed JH, & Edidin M (1989) Translational diffusion of class II major histocompatibility complex molecules is constrained by their cytoplasmic domains. *J. Cell Biol.* 109(6):3325-3331.

49. Klein L, Kyewski B, Allen PM, & Hogquist KA (2014) Positive and negative selection of the T cell repertoire: what thymocytes see (and don't see). *Nat. Rev. Immunol.* 14(6):377-391.

50. Rossjohn J, Pellicci DG, Patel O, Gapin L, & Godfrey DI (2012) Recognition of CD1d-restricted antigens by natural killer T cells. *Nature Reviews Immunology* 12(12):845-857.

51. Fox LM*, et al.* (2009) Recognition of lyso-phospholipids by human natural killer T lymphocytes. *PLoS biology* 7(10):e1000228.

52. Barral DC & Brenner MB (2007) CD1 antigen presentation: how it works. *Nature Reviews Immunology* 7(12):929-941.

53. Kang S-J & Cresswell P (2004) Saposins facilitate CD1d-restricted presentation of an exogenous lipid antigen to T cells. *Nat. Immunol.* 5(2):175-181.

54. Sergé A, Bertaux N, Rigneault H, & Marguet D (2008) Dynamic multiple-target tracing to probe spatiotemporal cartography of cell membranes. *Nat. Methods* 5(8):687-694.

55. Kusumi A, Sako Y, & Yamamoto M (1993) Confined Lateral Diffusion of Membrane-Receptors as Studied by Single-Particle Tracking (Nanovid Microscopy) - Effects of Calcium-Induced Differentiation in Cultured Epithelial-Cells. *Biophys J* 65(5):2021-2040.

Figure Legends

Figure 1. The actin cytoskeleton affects the mobility of hCD1d molecules on the surface of APCs.
(A) Schematic illustration of the labeling procedure. (Left) α-GalCer loaded hCD1d molecules (blue) were labeled using a conjugate of an iNKT-TCR (light and dark green) and a QD (red). (Right) Unpulsed hCD1d molecules were labeled using a monovalent anti-CD1d42 Ab conjugated to a QD. Not to scale. **(B)** Selected TIRFM image of the ventral side of a α-GalCer pulsed THP-1 cell displaying individual iNKT-TCR-QD-labeled hCD1d molecules (red) on the cell membrane. Representative 2D trajectories (white) are overlaid on the raw image (frame rate=100 Hz). **(C)** Distributions of the D_{2-4} values of α-GalCer loaded hCD1d labeled with the iNKT-TCR-QD conjugate or with Fab9b-Atto647N. **(D-F)** Distributions of the D_{2-4} values for α-GalCer-pulsed (*D*), unpulsed (*E*) and Gal-GalCer loaded hCD1d (*F*) THP-1 cells treated with 10 µM CytoD or expressing TD-hCD1d mutant molecules. Note that the comparisons of D_{2-4} values are always made with respect to the basal situation (DMSO) and specifically for each lipid-loaded condition, since the basal diffusion of hCD1d depends on the lipid. Data are representative from typically 200 trajectories per condition (90 trajectories in the case of hCD1d labeled with Fab9b-Atto647N) from at least 25 cells over 8 different experiments. *p<0.0001, ns: not significant (p>0.05) (one-way ANOVA test).

Figure 2. hCD1d molecules form nanoclusters on the surface of APCs whose properties depend on actin cytoskeleton interactions. (A) STED images of α-GalCer pulsed (upper row), Gal-GalCer pulsed (middle row) and unpulsed (lower row) THP-1 cells transfected with WT-hCD1d (left) or TD-hCD1d (right) mutant. Cells were stretched onto PLL-coated coverslips and labeled with anti-CD1d42 Ab. **(B,E,H)** Cluster size distribution, **(C,F,I)** distribution of the number of hCD1d molecules per cluster and **(D,G,J)** scatterplots of number of hCD1d molecules per cluster *vs.* cluster area corresponding to the quantification of the STED images. STED nanoscopy data are representative from at least 43 different images per condition, of 3x3 µm in size from at least 2 different experiments. Horizontal bars correspond to median values. *p<0.01 and **p<0.0001 (one-way ANOVA test).

Figure 3. The actin cytoskeleton regulates dynamic interactions between α-GalCer loaded hCD1d nanoclusters. (A) Schematic illustration of two α-GalCer loaded hCD1d molecules (blue) labeled with two different iNKT-TCR-QD-conjugates (green and red) at equimolar concentrations. Not to scale. **(B)** Magnified dual-color TIRFM images (1.9 µm in size) displaying two diffusing hCD1d nanoclusters over time, for the control case (left column), CytoD treated samples (middle column) and the TD-hCD1d mutant (right column). White arrows indicate the starting time of the interaction. **(C)** Representative dual-color trajectories of two different hCD1d nanoclusters reconnected over a total observation time of 1s (frame rate: 30 Hz). **(D)** Separation distances of two α-GalCer loaded hCD1d nanoclusters over time for untreated WT–hCD1d (green), CytoD treated WT-hCD1d (red) and the TD-hCD1d mutant (blue). **(E)** Distributions of the interparticle distances from experimental data (color dots) together with Monte Carlo simulations of random encounters (gray dots). Data are representative of at least 20 different trajectories on 9 different cells per condition over 6 different experiments. *p<0.05 and **p<0.0001 (one-way ANOVA test).

Figure 4. The actin cytoskeleton actively arrests diffusing α-GalCer loaded hCD1d nanoclusters on the cell membrane. (A) Snapshot of a dual-color TIRFM movie displaying lifeact-GFP labeled actin
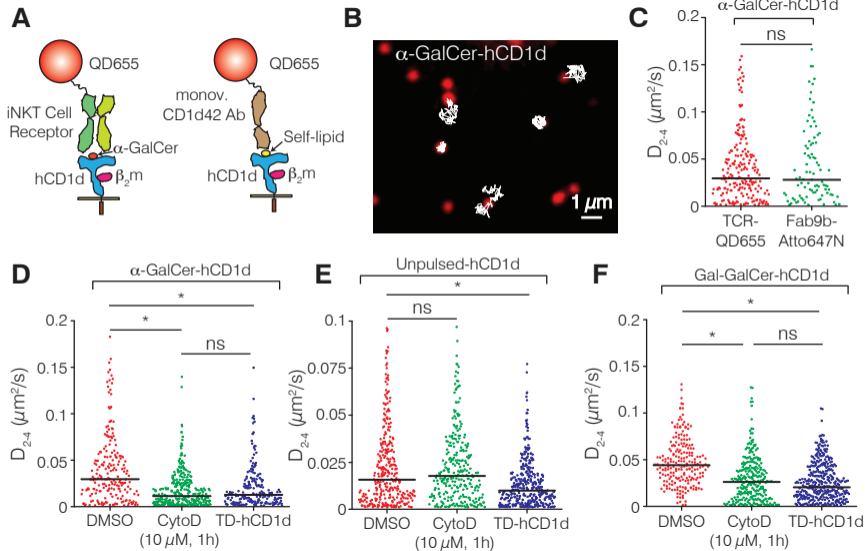
(green) and α-GalCer loaded hCD1d nanoclusters (red) labeled with the iNKT-TCR-QD conjugate. Scale bar: 2 μm. **(B,C)** Representative magnified TIRFM images at two different time sequences with an example of a 2D trajectory of α-GalCer loaded hCD1d diffusing inside (black line) and outside (white line) actin-rich regions, with the diffusing particle outlined with a red-dashed circle. In panel **(B)** hCD1d is inside actin, while **(C)** shows the time sequence when hCD1d is outside actin. Scale bar: 500 nm. **(D)** Distributions of the D_{2-4} values for α-GalCer loaded WT-hCD1d and α-GalCer loaded TD-hCD1d nanoclusters inside and outside high-actin regions. The D_{2-4} values reported here are somewhat different as to the median values reported in the corresponding Fig. 1, as a pre-selected number of trajectories that diffused outside and inside actin-rich regions were chosen for this analysis. **(E,F)** Cumulated cartography maps containing 8000 localizations over a recording time of 20s from α-GalCer loaded WT-hCD1d **(E)** and TD-hCD1d **(F)** overlaid onto a lifeact-GFP TIRFM image. The white dots correspond to the different spatial positions explored by hCD1d during the observation time. The pseudo-colored image corresponds to the actin intensity, going from blue (actin-low) to red (actin-rich). The black filled arrows point to hCD1d diffusion on actin-poor regions, whereas empty-black arrows point to hCD1d diffusing close to actin-rich regions. Scale bar: 1 μm **(G)** Fractional occurrence of hCD1d localization positions *vs.* changes in actin intensity, ΔActin for α-GalCer loaded WT-hCD1d (black) and α-GalCer loaded TD-hCD1d (red). Data were fitted with a straight line and the slope was obtained. SPT data from at least 87 trajectories on 30 different cells over 5 different experiments. Cartography maps data contain at least 8000 localizations. Analysis has been performed on 6 different cells and 3 different experiments per condition. *p<0.0001 (Student's t-test).

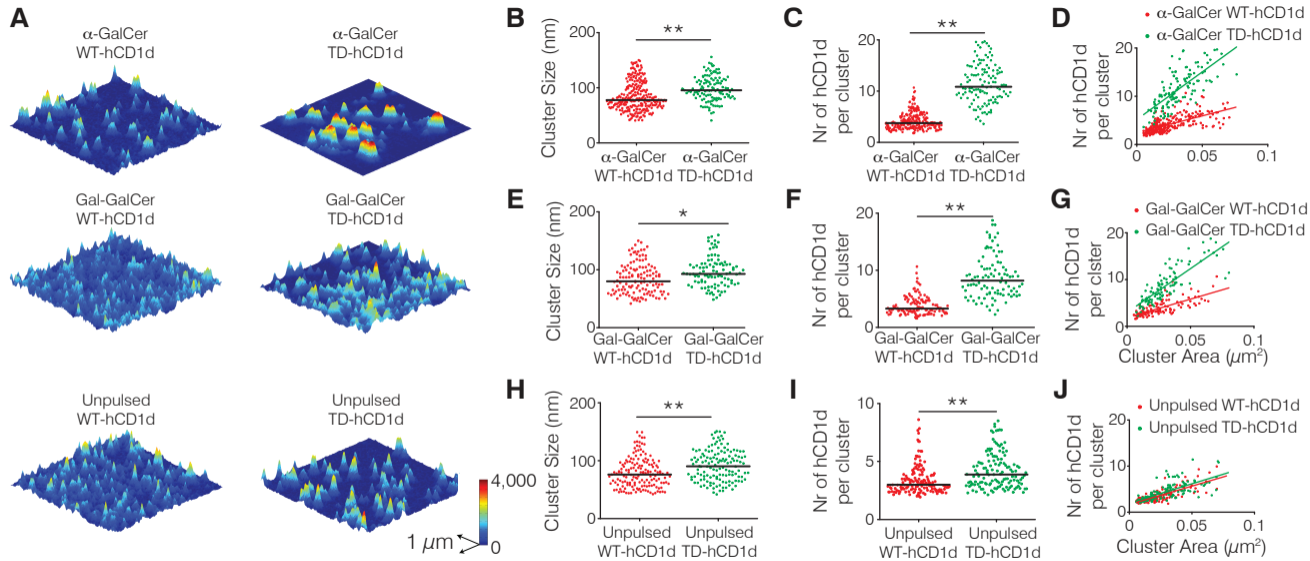**Figure 5. Perturbation of the actin cytoskeleton on α-GalCer pulsed APCs enhances iNKT cell activation. (A,B)** IFN-γ production upon iNKT cell activation by **(A)** hCD1d transduced THP1 cells or **(B)** immature dendritic cells (imDCs), pulsed with the given α-GalCer concentrations overnight before treatment with Cyto D. **(C)** Expression levels of hCD1d as measured by FACS after treating THP1 cells with CytoD (10 μM, 1h). **(D)** IFN-γ production upon iNKT cell activation by hCD1d THP1 cells stimulated with 10 μg/ml of TLR 7/8 ligand R848 for 30h before CytoD treatment. The unpulsed column refers to no lipid. (•) Intensity value below the detection limit. Data are representative of 3 different experiments. *p<0.05, ns: not significant (p>0.05) (Student's t-test).
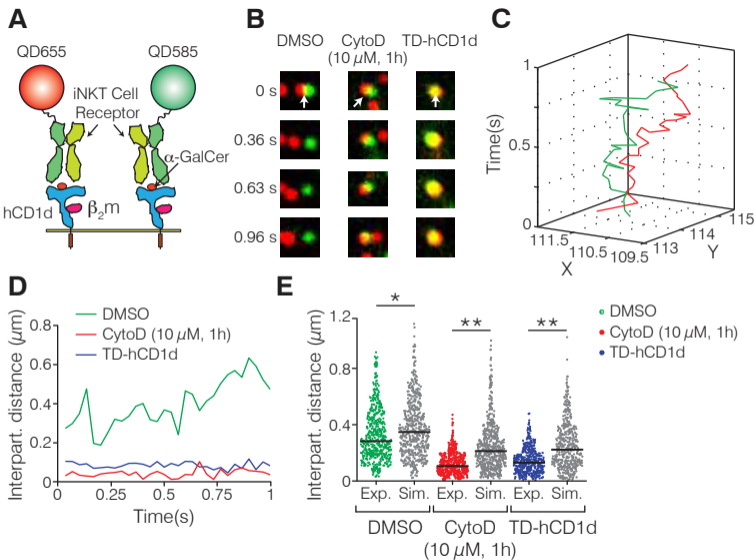
Figure 6. The actin cytoskeleton regulates hDC1d nanoclustering under inflammatory conditions. (A) STED images of unpulsed WT-hCD1d (upper row), R848-WT-hCD1d (middle row) and R848-TD-hCD1d (lower row) on the dorsal cell membrane of THP-1 cells stretched on PLL-coated glass coverslips. **(B,E)** Distributions of cluster size; **(C,F)** distribution of the number of hCD1d molecules per cluster; and **(D,G)** scatterplots of the number of hCD1d molecules per cluster *vs.* cluster area corresponding to the quantification of the STED images. STED nanoscopy analysis data from at least 30 different images of 3x3 μm in size, from at least 2 different experiments. Horizontal bars correspond to median values. *p<0.0001 (one-way ANOVA test).
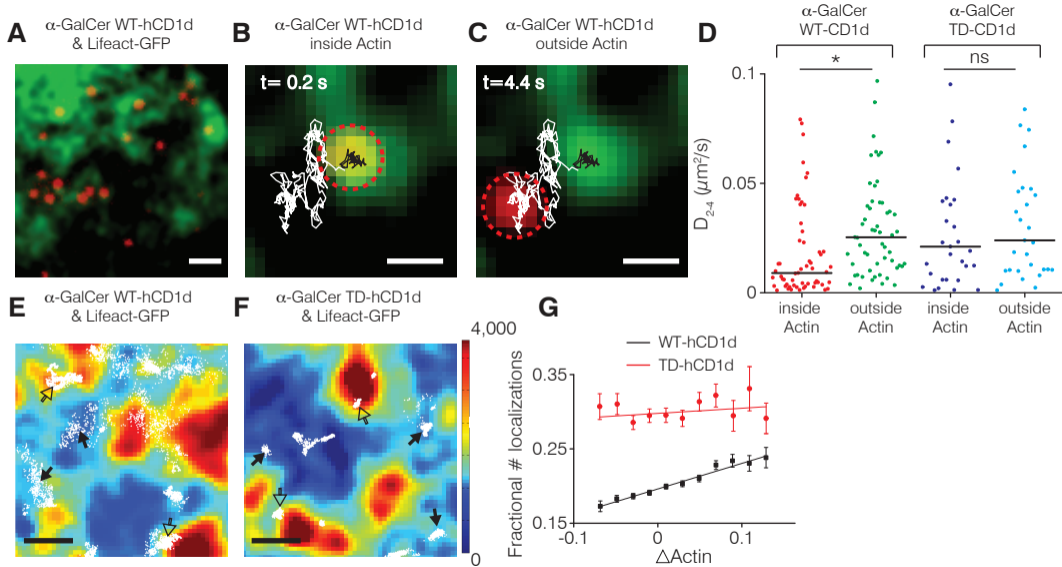
Figure 7. The actin cytoskeleton controls CD1d nanoclustering on the surface of APCs, fine-tuning iNKT activation. (A) Small basal nanoclusters of stimulating-lipid loaded-CD1d molecules are present on the cell membrane of APCs. Barriers and/or obstacles by the actin cytoskeleton keep CD1d nanoclusters away from each other limiting their aggregation state, regulating in turn iNKT cell
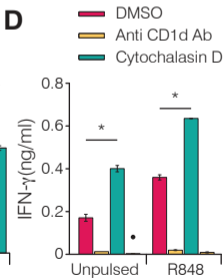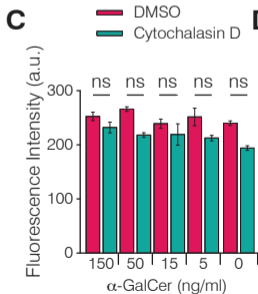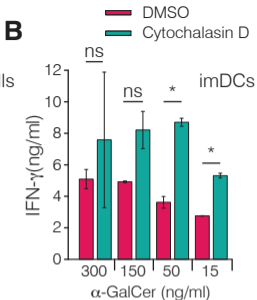
activation even under inflammatory conditions ("iNKT cell autoreactivity"). (*B*) Re-arrangement of the actin cytoskeleton (achieved in our case by the use of CytoD treatment) increases the encountering rate between CD1d-1d nanoclusters, resulting in the formation of larger lipid-loaded CD1d nanoclusters and increased iNKT cell activation.

A

α-GalCer
WT-hCD1d

α-GalCer
TD-hCD1d

Gal-GalCer
WT-hCD1d

Gal-GalCer
TD-hCD1d

Unpulsed
WT-hCD1d

Unpulsed
TD-hCD1d

1 μm

4,000

0

B

Cluster Size (nm)

**

α-GalCer
WT-hCD1d   α-GalCer
TD-hCD1d

C

Nr of hCD1d per cluster

**

α-GalCer
WT-hCD1d   α-GalCer
TD-hCD1d

D

Nr of hCD1d per cluster

α-GalCer WT-hCD1d
α-GalCer TD-hCD1d

E

Cluster Size (nm)

*

Gal-GalCer
WT-hCD1d   Gal-GalCer
TD-hCD1d

F

Nr of hCD1d per cluster

**

Gal-GalCer
WT-hCD1d   Gal-GalCer
TD-hCD1d

G

Nr of hCD1d per clster

Gal-GalCer WT-hCD1d
Gal-GalCer TD-hCD1d

Cluster Area (μm^2)

H

Cluster Size (nm)

**

Unpulsed
WT-hCD1d   Unpulsed
TD-hCD1d

I

Nr of hCD1d per cluster

**

Unpulsed
WT-hCD1d   Unpulsed
TD-hCD1d

J

Nr of hCD1d per cluster

Unpulsed WT-hCD1d
Unpulsed TD-hCD1d

Cluster Area (μm^2)

A QD655 QD585

iNKT Cell Receptor

α-GalCer

hCD1d β₂m

B DMSO | CytoD (10 μM, 1h) | TD-hCD1d

0 s
0.36 s
0.63 s
0.96 s

C Time(s) X Y

D

Interpart. distance (μm)

— DMSO
— CytoD (10 μM, 1h)
— TD-hCD1d

Time(s)

E

Interpart. distance (μm)

*

**

**

Exp. Sim. | Exp. Sim. | Exp. Sim.

DMSO | CytoD (10 μM, 1h) | TD-hCD1d

● DMSO
● CytoD (10 μM, 1h)
● TD-hCD1d

A α-GalCer WT-hCD1d & Lifeact-GFP

B α-GalCer WT-hCD1d inside Actin — t= 0.2 s

C α-GalCer WT-hCD1d outside Actin — t=4.4 s

D α-GalCer WT-CD1d   α-GalCer TD-CD1d

D_{2-4} $(\mu m^2/s)$

inside Actin   outside Actin   inside Actin   outside Actin

E α-GalCer WT-hCD1d & Lifeact-GFP

F α-GalCer TD-hCD1d & Lifeact-GFP

G Fractional # localizations vs ΔActin

WT-hCD1d
TD-hCD1d

A

DMSO
Cytochalasin D

THP1 cells

IFN-γ(ng/ml)

ns   ns

$\ast$

$\ast$

α-GalCer (ng/ml)
150   50   15   5

B

DMSO
Cytochalasin D

imDCs

IFN-γ(ng/ml)

ns   ns $\ast$

$\ast$

α-GalCer (ng/ml)
300   150   50   15

C

DMSO
Cytochalasin D

Fluorescence Intensity (a.u.)

ns   ns   ns   ns   ns

α-GalCer (ng/ml)
150   50   15   5   0

D

DMSO
Anti CD1d Ab
Cytochalasin D

IFN-γ(ng/ml)

$\ast$

$\ast$

Unpulsed   R848

A

Unpulsed
WT-hCD1d

R848
WT-hCD1d

R848
TD-hCD1d

4,000

0 — 1 μm

B

Cluster Size (nm)

Unpulsed WT-hCD1d   R848 WT-hCD1d

*

C

Nr of hCD1d per cluster

Unpulsed WT-hCD1d   R848 WT-hCD1d

*

D

Nr of hCD1d per cluster

• Unpulsed WT-hCD1d
• R848-WT-hCD1d

Cluster Area (μm²)

E

Cluster Size (nm)

R848 WT-hCD1d   R848 TD-hCD1d

*

F

Nr of hCD1d per cluster

R848 WT-hCD1d   R848 TD-hCD1d

*

G

Nr of hCD1d per cluster

• R848-WT-hCD1d
• R848-TD-hCD1d

Cluster Area (μm²)

A

IFN-γ   IFN-γ

iNKT cell

iNKT-TCR

iNKT cell
stimulating lipid

CD1d

Actin Cytoskeleton   APC

B

IFN-γ   IFN-γ   IFN-γ   IFN-γ

iNKT cell

APC